Quasi-linear MHD modelling of H-mode plasma response to resonant magnetic perturbations

E. Nardon[1]**, P. Tamain**[1]**, M. Bécoulet**[2]**, G. Huysmans**[2] **and F.L. Waelbroeck**[3]

[1] Euratom/UKAEA Fusion Association, Culham Science Centre, Abingdon, Oxon OX14 3DB, UK
[2] Association Euratom/CEA, CEA Cadarache, F-13108, St. Paul-lez-Durance, France
[3] Institute for Fusion Studies, University of Texas, Austin, TX 78712, USA

E-mail: eric.nardon@ukaea.org.uk

Abstract

The plasma response to externally imposed resonant magnetic perturbations (RMPs) is investigated through quasi-linear MHD modelling in the case where the resonant surfaces are located in the pedestal of an H-mode plasma. The pedestal is a particular region regarding the question of plasma response to RMPs because of its strong $E \times B$ and electron diamagnetic rotations. It is found that a strong rotational screening takes place in most of the pedestal. The RMPs may, however, penetrate in a narrow layer at the very edge, where the plasma is cold and resistive. The possibility that one harmonic of the RMPs may also penetrate if its resonant surface is at a particular location, close to the top of the pedestal, where the $E \times B$ and electron diamagnetic rotations compensate each other, is discussed. Finally, the RMPs are found to produce some additional transport, even though they do not penetrate.

PACS numbers: 52.30.Ex, 52.35.Vd, 52.55.Fa, 52.55.Tn, 52.65.Kj

(Some figures in this article are in colour only in the electronic version)

1. Introduction

The results of successful experiments on edge localized modes (ELMs) control by externally imposed resonant magnetic perturbations (RMPs) have generated an interest in understanding the MHD response of an H-mode plasma to external RMPs. In such experiments (for instance at DIII-D [1, 2] and JET [3, 4]), a set of coils is used in order to produce radial magnetic perturbations which, according to the vacuum modelling (where the plasma response is neglected), create magnetic islands on the resonant surfaces. The high radial density of resonant surfaces resulting from the large edge magnetic shear of X-point plasmas facilitates the overlap of vacuum islands at the edge, resulting in a stochastic region. The stochastization of the magnetic field at the edge is often presented as a possible mechanism of the observed ELM suppression or mitigation. However, the validity of the vacuum approach can be questioned. In particular, we address here the question of the so-called 'rotational screening' of the RMPs, taking parameters which are typical for the DIII-D ELM control experiments using the I-coils.

The rotational screening of RMPs results from the motion of the electron fluid across the field lines at the resonant surfaces [5–7]. Indeed, in the presence of such a motion, static RMPs in the laboratory frame correspond to time-varying RMPs in the electron fluid frame, and therefore induce an electron current opposing their penetration (i.e. hindering reconnection). The velocity of the electron fluid across the field lines can be written as $V_{\perp e} = V_E + V_{*e}$, where $V_E = E_r/B$ is the $E \times B$ drift velocity and $V_{*e} = p'_e/en_e B$ is the electron diamagnetic drift velocity (the prime denotes the radial derivative). The radial electric field E_r can itself be decomposed in the following way (as a consequence of the radial force balance for the ions): $E_r = V_{\theta i} B_\varphi - V_{\varphi i} B_\theta - V_{*i} B$, where $V_{\theta i}$ and $V_{\varphi i}$ are the ion fluid poloidal and toroidal velocities and $V_{*i} = -p'_i/Z_i en_e B$ is the ion diamagnetic drift velocity.

Fitzpatrick [8, 9] has developed a theory of the response of rotating plasma to external RMPs originally in a core plasma situation, where E_r is dominated by the toroidal rotation term $-V_{\varphi i} B_\theta$ and where the diamagnetic effects are small because $|V_E| \gg |V_{*e}|$. In this case, the screening is essentially due

to the toroidal rotation. The case of interest in this paper is different. Indeed, in the pedestal of an H-mode plasma, the composition of E_r is more complex and involves an order zero contribution from the diamagnetic term $-V_{*i}B$ due to the strong pressure gradient. Furthermore, V_E and V_{*e} are of the same order. It is therefore essential, in order to address the question of rotational screening in the pedestal, to retain the diamagnetic effects.

Let us now briefly review the previous attempts to model the plasma response to the I-coils in the DIII-D ELM control experiments. Bécoulet *et al* [10] applied the analytical expression from the Fitzpatrick theory [8, 9] for the screening factor due to the toroidal rotation, neglecting the diamagnetic effects. As discussed above, this is valid to leading order in the core but not in the pedestal. Similarly, non-linear MHD simulations in realistic geometry such as reported in [11] using the JOREK code, miss the diamagnetic effects. More recently, other simulations of this type using the NIMROD [12] and M3D codes [13], included diamagnetic effects to some extent without, however, using the correct profiles in the pedestal. Furthermore, all such realistic geometry simulations [11–13] need to be run with a resistivity much larger than the experimental one, for numerical reasons. Since resistivity is an essential parameter in the screening physics, these codes cannot model properly the rotational screening. To the best of our knowledge, the only published work that includes the diamagnetic effects and uses a realistic resistivity is by Heyn *et al* [14]. They employ a linear kinetic model in cylindrical geometry, taking the profiles for toroidal rotation, electron density and temperature from a DIII-D discharge from the ELM control experiments. They find a rather strong screening of the RMPs at virtually every resonant surface across the plasma, except at the very edge. Our purpose here is to address the problem using a fluid model instead of a kinetic one, while retaining some important quasi-linear effects. We should mention that Reiser and Chandra [15], as well as Yu *et al* [5–7], already applied non-linear fluid models, somewhat similar to the one we use here, in order to study the question of RMPs screening by plasma response. However, unlike the above-mentioned references and this work, their work was done for TEXTOR parameters instead of DIII-D parameters and for L-mode rather than H-mode (no pressure pedestal and E_r well were included), which justifies the interest of this paper.

In section 2, we describe our model and discuss its relevance and limitations. In section 3, we present the results of a simulation with DIII-D-like parameters, attempting to model the ELM control experiments using the I-coils. In section 4, we discuss the results. Finally, we summarize and conclude in section 5.

2. Model

2.1. Geometry, equations, normalizations

As in [10, 14], we work in cylindrical geometry. We thus lose realistic geometry, in exchange for which we are able to include a realistic resistivity. We also neglect toroidal curvature, but it should be kept in mind that, as shown in [15], curvature effects play a quantitative role in the screening physics: they tend to increase the screening efficiency. Since, as shown in section 3,

we find that a strong screening occurs, we may assume that the inclusion of curvature effects would reinforce our conclusions. We use the four-field reduced MHD model taken from [16], assuming cold ions ($\tau \equiv T_i/T_e = 0$), neglecting electron inertia and including diffusive terms that are omitted in [16]:

$$\partial_t U + [\phi, U] + \nabla_\| J = \nu_\perp \Delta_\perp (U - U_0), \quad (1)$$

$$\partial_t \psi + \nabla_\|(\phi - \delta p) = \eta(J - J_0), \quad (2)$$

$$\partial_t p + [\phi, p] + \beta \nabla_\|(V + 2\delta J) = \chi_\perp \Delta_\perp (p - p_0), \quad (3)$$

$$\partial_t V + \tfrac{1}{2}\nabla_\| p + [\phi, V] = \nu_\| \Delta_\perp (V - V_0). \quad (4)$$

Here, $U \equiv \Delta_\perp \phi$ is the vorticity projected along the z-axis (which is the equivalent of the toroidal direction in cylindrical geometry), ϕ is the electrostatic potential, $\nu_\perp$ is the perpendicular viscosity, ψ is the poloidal magnetic flux, $\delta \equiv (c/2\omega_{pi})/a$ (where c is the speed of light, $\omega_{pi} \equiv (n_e e^2/\varepsilon_0 A_i m_i)^{1/2}$ and a is the minor radius) parametrizes the finite Larmor radius effects, p is the pressure, η is the resistivity, $J \equiv \Delta_\perp \psi$ is the current density projected along the z-axis, $\beta \equiv p/(B_0^2/2\mu_0)$ (B_0 being the toroidal field), $\chi_\perp$ is the perpendicular heat diffusivity (the inclusion of parallel heat diffusion is left for future work), V is the parallel (to the equilibrium field lines) velocity and $\nu_\|$ is the parallel viscosity. We remark that δ and β are taken as parameters, calculated from the top of the pedestal density and pressure, but the model would be more accurate if they had a profile. The Poisson brackets are defined by $[A, B] = \vec{e}_z \cdot \vec{\nabla} A \times \vec{\nabla} B$. The parallel gradient is defined as $\nabla_\| A = \partial_z A + [A, \psi]$, parallel thus referring here to the total magnetic field, including perturbations. The perpendicular Laplace operator is defined, in our cylindrical coordinates system (r, z, θ), as $\Delta_\perp A = (1/r)\partial_r(r\partial_r A) + (1/r^2)\partial_{\theta\theta}^2 A$. We use source terms $-\nu_\perp \Delta_\perp U_0$, $-\eta J_0$, $-\chi_\perp \Delta_\perp p_0$ and $-\nu_\| \Delta_\perp V_0$ to compensate for the diffusion of the equilibrium profiles U_0, J_0, p_0 and V_0. All distances are normalized to the minor radius a, time is normalized to the Alfvén time $\tau_A \equiv a/V_A \equiv a/(B_0/(\mu_0\rho_0)^{1/2})$, magnetic flux to aB_0 and current density to $B_0/\mu_0 a$. In (1), the viscosity appears in the normalized form $\nu_\perp \equiv Re^{-1} \equiv \tau_A/\tau_V$, where Re is the Reynolds number and τ_V is the viscous time defined by $\tau_V \equiv a^2/\nu_{\perp[m^2 s^{-1}]}$, where $\nu_{\perp[m^2 s^{-1}]}$ is the actual viscosity in m² s⁻¹. Similarly, in (2) the resistivity appears in the normalized form $\eta \equiv S^{-1} \equiv \tau_A/\tau_R$, where S is the Lundquist number and τ_R is the resistive time defined by $\tau_R \equiv \mu_0 a^2/\eta_{[\Omega m]}$, where $\eta_{[\Omega m]}$ is the actual resistivity in Ωm.

We note that the $\nabla_\|(\phi - \delta p)$ term in equation (2) contains a $(V_E + V_{*e}) \cdot \partial_\theta \psi$ part which is the origin of the screening currents due to the rotation.

2.2. Numerical implementation

The system (1)–(4) is solved using the 4FC 4-field cylindrical MHD code. 4FC solves the complete equations of the model described in [16], but is run here with the τ parameter set equal to zero to work with cold ions ($T_i/T_e = 0$). Diffusion terms have been added for the equilibrium drive, as described above. The equations are discretized along the radial direction following a finite differences approach based on a user-defined
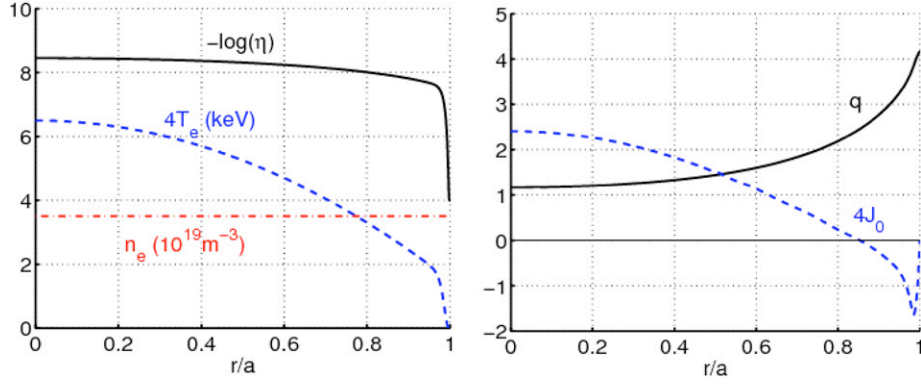
Figure 1. Left: input density, electron temperature and normalized resistivity profiles. Right: initial normalized current profile and q profile.

non-uniform mesh $(r_k)_{k=1,...,Nr}$. The two periodical directions (poloidal and 'toroidal') are treated in the Fourier space:

$$X(r, \theta, \zeta) = \sum_{m,n \in E_{mn}} \tilde{X}_{mn}(r) \cdot \exp(\mathrm{i}(m\theta - n\zeta)),$$

where $\zeta \equiv 2\pi(z/R_0)$, X is one of the unknown fields and E_{mn} is a user-defined set of modes to be treated (where m and n are the poloidal and toroidal mode numbers). For simplicity, the tildes will be omitted in the rest of the paper. A semi-implicit method is applied for the time-stepping: while linear terms (diffusion terms and toroidal gradient terms) are treated implicitly, the non-linear contribution of the Poisson brackets operator, which is responsible for the modes interaction, is treated explicitly.

2.3. Boundary conditions (BCs) and model for the externally imposed RMPs

For the BCs, we set

- for the $(m, n) = (0, 0)$ 'equilibrium' harmonic: $U'_{00}|_{r=0} = U_{00}|_{r=1} = 0$, and similarly for J_{00}, p_{00}, V_{00}, ϕ_{00} and ψ_{00};
- for the $(m, n) \neq (0, 0)$ 'perturbation' harmonics: $U_{mn}|_{r=0} = U_{mn}|_{r=1} = 0$, and similarly for J_{mn}, p_{mn}, V_{mn}, ϕ_{mn} and $\psi_{mn}|_{r=0}$. The only exception is for ψ_{mn} at $r = 1$. Indeed, the external RMPs are imposed through the BC: $\psi'_{mn}|_{r=1} = m\lfloor 2\psi_{mn}^{\mathrm{vac}} - \psi_{mn}|_{r=1}\rfloor$. This represents a current distribution in the z-direction with an (m, n) symmetry, localized on a cylinder of radius $r_{\mathrm{coils}} \geqslant 1$ and producing, in vacuum, an (m, n) poloidal flux $\psi_{mn} = \psi_{mn}^{\mathrm{vac}}$ at $r = 1$ (see the demonstration in the appendix). This is an exact BC if the plasma is surrounded by a perfect vacuum without any wall. It is more physical than imposing the value of ψ_{mn} at $r = 1$, in the sense that it represents the effect of a current distribution (i.e. coils) instead of that of a prescribed magnetic perturbation at the boundary. We model the $n = 3$ perturbations from the I-coils by imposing, for each resonant harmonic, a vacuum radial resonant field (normalized to the toroidal field) giving an RMP field on the resonant surface of $b_{mn}^{\mathrm{r}} = 4 \times 10^{-4}$. The latter value is a typical one for the DIII-D I-coils, taken from [17]. In terms of our BCs, this corresponds to $\psi_{mn}^{\mathrm{vac}} = r_{mn}^{-m+1} b_{mn}^{\mathrm{r}}/m$, where r_{mn} is the radius of the resonant surface. The RMPs are switched on at the beginning of the simulation over $\sim 2\tau_{\mathrm{A}}$, i.e. we use $\psi_{mn}^{\mathrm{vac}}(t) = (r_{mn}^{-m+1} b_{mn}^{\mathrm{r}}/m)(1 - \mathrm{e}^{-t/2\tau_{\mathrm{A}}})$.

2.4. Limitations of the model

The physics of rotation and radial electric field in the pedestal of an H-mode plasma [18] involves an interplay between the neoclassical damping of the poloidal rotation [19], ion orbit losses [20], turbulence-driven zonal flows [21], etc. It is also known that a stochastic magnetic field at the edge increases the radial electric field [22–24]. None of these phenomena, which are potentially crucial, is modelled in this work. Our model can therefore not pretend to be complete and our ambition is limited to showing some of the important mechanisms which are at play in the physics of the H-mode plasma response to external RMPs.

2.5. Input parameters and profiles

The parameters are DIII-D-like: minor radius $a = 0.6$ m, major radius $R_0 = 1.70$ m, vacuum toroidal field on axis $B_0 = 1.95$ T. The electron density is considered flat, with the value $n_{\mathrm{e}} = 3.5 \times 10^{19}$ m^{-3}. The electron temperature profile has a pedestal of ~ 500 eV of height and $\sim 2\%$ of width in normalized radius. We use a Spitzer–Härm [25] resistivity profile, calculating η from T_{e}: $\eta_{[\Omega m]} = 2.8 \times 10^{-8}/T_{\mathrm{e}\,[\mathrm{keV}]^{3/2}}$. Figure 1 presents the n_{e}, T_{e} and η input profiles. The Alfvén time with these parameters is $\tau_{\mathrm{A}} = 1.2 \times 10^{-7}$ s and the Alfvén velocity $V_{\mathrm{A}} = 5.0 \times 10^6$ m s^{-1}.

We derive the initial vorticity profile U_0 from the radial electric field profile. For the latter, we use an analytical expression in which we set the parameters in order to resemble the profile deduced from charge exchange radiation spectroscopy measurements for C VI ions for DIII-D shot 122481 at ~ 1900 ms, which is shown in figure 6(*b*) of [26]. The initial profiles of the $E \times B$ velocity and electron diamagnetic velocity, together with their sum (i.e. the total poloidal electron velocity), are shown in figure 2 (left).

The current profile J_0 is calculated from a q profile representative of a typical DIII-D H-mode, with $q_{95} \sim 3.6$. One drawback of the cylindrical modelling is that an unrealistic large negative current density at the edge is needed in order to obtain the large magnetic shear due to the X-point in DIII-D (Heyn *et al* met the same difficulty [14]). In other words, a compromise has to be made between the current profile and the q profile in a cylindrical modelling: both cannot be reproduced at the same time. Here, we choose to privilege the q profile. In order to satisfy the BC $J_0|_{r=1} = 0$, we cannot, however,
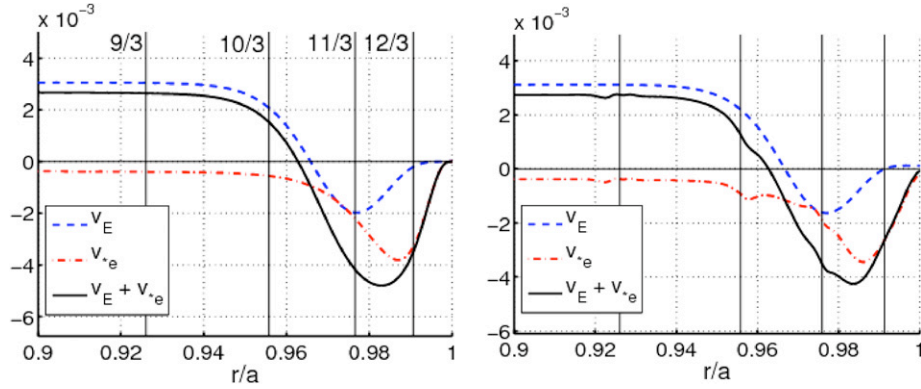
Figure 2. Initial (left) and final (right) rotation profiles (velocities are normalized to the Alfvén velocity). The vertical lines show the position of the resonant surfaces (where $q = m/3$).

reproduce the divergence of q at the separatrix. The current and q profiles are shown in figure 1 (right).

The other parameters are $\beta = 2.76 \times 10^{-3}$, $\nu_\perp = \nu_\parallel = 2 \times 10^{-6}$ (corresponding to $\sim 6\,\text{m}^2\,\text{s}^{-1}$) and $\chi_\perp = 5 \times 10^{-8}$ (corresponding to $\sim 0.15\,\text{m}^2\,\text{s}^{-1}$). It can be remarked that the viscosity is taken larger than the typical anomalous viscosity (which would be $\sim 1\,\text{m}^2\,\text{s}^{-1}$). We are, however, constrained to use such a large value in order to start the simulations with an intrinsically stable plasma. Indeed, at low viscosity, a simulation without any external RMPs shows that the (11, 3) mode is tearing unstable. For the heat diffusivity $\chi_\perp$, however, we are able to use a value which is typical of the neoclassical transport taking place in the pedestal. Thus, the extra heat transport induced by the RMPs in the pedestal can directly be compared with a realistic level of background transport.

We do not impose an experimental parallel rotation profile and instead we simply use $V_0 = 0$. We indeed believe that the parallel rotation does not play an important role in the physics addressed here (in particular, it does not appear in equation (2), which governs the rotational screening through the $\nabla_\parallel (\phi - \delta p)$ term).

2.6. Numerical parameters

We use a non-equidistant radial mesh with 150 grid points, $\sim 3/4$ of which are located between $r = 0.9$ and $r = 1$. The time step is of $4 \times 10^{-2} \tau_\text{A}$. Only the harmonics $(m, n) = (0, 0)$, $(9, 3)$, $(10, 3)$, $(11, 3)$ and $(12, 3)$ are considered. The positions of the resonant surfaces can be seen in figure 2. The simulations are quasi-linear in the sense that the perturbation harmonics can, by interacting with themselves, modify the $(0, 0)$ profiles. The perturbation harmonics interact between each other only through the $(0, 0)$ mode.

3. Results

The simulation is run for $8 \times 10^3 \tau_\text{A}$, until a steady state is reached. Figure 3 shows the final profiles of the poloidal flux for the different perturbation harmonics. The profiles for the vacuum field are also shown for comparison. It is notable that for all but the (12, 3) harmonic, ψ_{mn} goes almost exactly to 0 at the position of the corresponding resonant surface. This means that very little reconnection takes place, i.e. there is a strong screening. Figure 4 (left) shows a Poincaré plot at the

end of the simulation. It can be compared with figure 4 (right), which presents a Poincaré plot in a simulation with E_r and δ both set to zero, i.e. where there is no rotation (neither $E \times B$ nor diamagnetic [remember that δ quantifies the finite Larmor radius effects]) and therefore no screening. As can be expected from the ψ_{mn} profiles, the only clearly observable island chain in figure 4 (left) is the (12, 3) one.

The fact that a partial penetration of the (12, 3) RMPs takes place may be attributed to the larger resistivity at the $q = 12/3$ surface, which is at the edge, where the plasma is colder. This indicates that, in reality, it is likely that there is a thin stochastic layer at the very edge of the plasma. However, in the present simulations, we cannot reproduce this effect because we are unable to reproduce the q profile at the very edge, as discussed above.

The strong screening for the (9–11, 3) modes is due to helical currents being induced by the RMPs, which are shown in figure 5. One can see that these currents have rather complicated profiles, but are essentially located around their respective resonant surfaces.

It can be seen by comparing figure 2 left and right that the V_{*e} profile is affected by the RMPs around the resonant surfaces. Figure 6 shows the pressure profile for the (0, 0) mode at the beginning of the simulation (this profile would maintain itself without the RMPs) and at the end of it. The visible difference is a reflection of the effect of the RMPs on the transport. Calculating the contribution of the different terms in the pressure equation, we found that the transport is essentially due to the $[\phi, p]$ term (i.e. to convection cells, which recalls [11, 12]) and to the $\beta \nabla_\parallel (2\delta J)$ term. It has been shown recently by Yu and Günter [5] that the $\beta \nabla_\parallel (2\delta J)$ term can produce transport, and thereby affect the diamagnetic rotation profile, in a similar way as the $\nabla_\parallel J$ term in the vorticity equation is known to affect the $E \times B$ rotation profile [8, 9]. It is argued in [5] that which one of the two rotation profiles (diamagnetic or $E \times B$) is most affected depends on the ratio of diffusivities $\chi_\perp / \nu_\perp$. In our case, $\nu_\perp \gg \chi_\perp$ and accordingly the effect is mainly on the diamagnetic rotation. The fact that the diamagnetic rotation profile is affected by the RMPs means that the RMPs induce, at least locally, a transport that is comparable to the background transport. This mechanism may account for the density pump-out observed in the experiments [1, 2]. It should be kept in mind that the parallel heat conduction, which
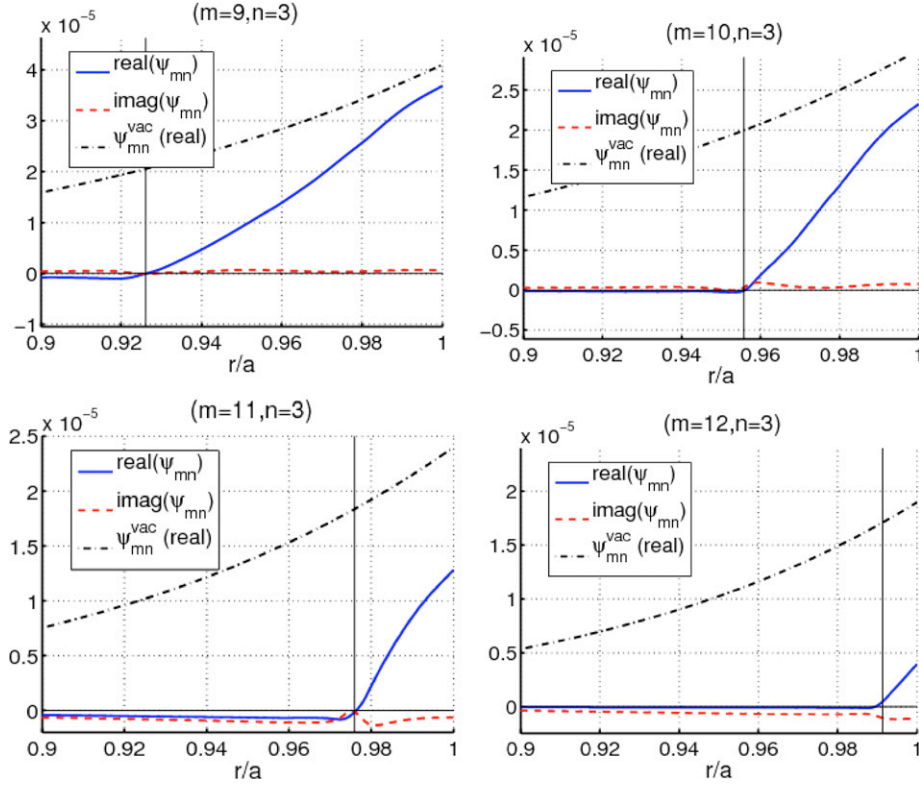
Figure 3. Final profile of the poloidal flux for each perturbation harmonic (real and imaginary parts). The position of the resonant surface is shown by the vertical line. The vacuum field (which only has a real part) is also shown.
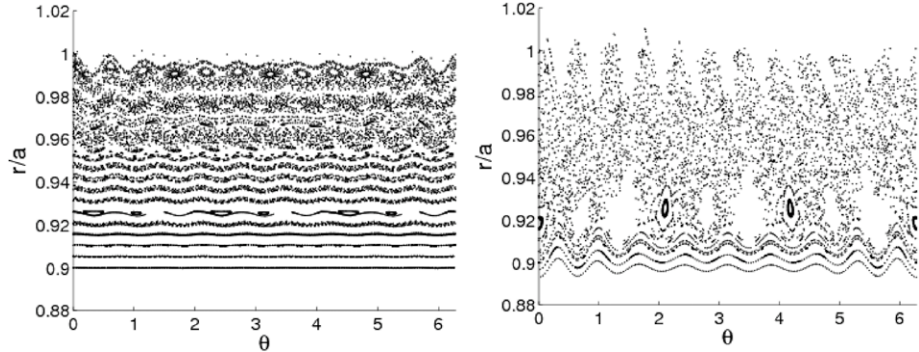

Figure 4. Poincaré plot at the end of the simulation. Left: with $E \times B$ and diamagnetic rotation. Right: without any rotation.

we have omitted here, may also play an important role in the transport.

Looking at the input rotation profiles of figure 2 (left) again, it is interesting to note that there exists a location, close to the top of the pedestal, where $V_{\perp e} = V_E + V_{*e} = 0$. If a resonant surface was located near this point, one could expect RMP penetration. To verify this, we did a simulation where we multiplied the equilibrium current profile by a factor 1.03. This way, the $q = 10/3$ surface coincided with the surface where $V_{\perp e} = 0$, as can be seen in figure 7 (top left). For simplicity, we simulated only the $(0, 0)$ and $(10, 3)$ modes. The simulation was run for a duration of $2 \times 10^4 \tau_A$. It can be seen in figure 7 (top right) that the RMPs indeed penetrate. Figure 7 (bottom left and right) shows that this is associated with a reduction in $|V_{*e}|$ (i.e. the pressure gradient) at $q = 10/3$, which is accompanied by a reduction in V_E, so that $V_{\perp e}$ remains small.

Although the reduction in $|V_{*e}|$ is localized, the reduction in V_E is rather global, which can be attributed to the large viscosity used in the simulation.

The scenario of an island chain penetrating at a surface located close to the pedestal top is an attractive one to explain the effect of the I-coils on the profiles, in particular the fact that the pressure gradient is mainly affected around the top of the pedestal (see figure 6(*g*) in [1]). It appears, however, to be incompatible with the experimentally observed effect of the I-coils on E_r. Indeed, figure 6(*b*) of [26] clearly shows that E_r increases in the presence of the I-coils, i.e. V_E increases, oppositely to the evolution observed in our simulation. Note, however, that in the previous simulation (see figure 2) E_r is increased slightly by the RMPs, in qualitative agreement with the experiment. In any case, the penetration of an island chain should in principle be testable experimentally, by analysing
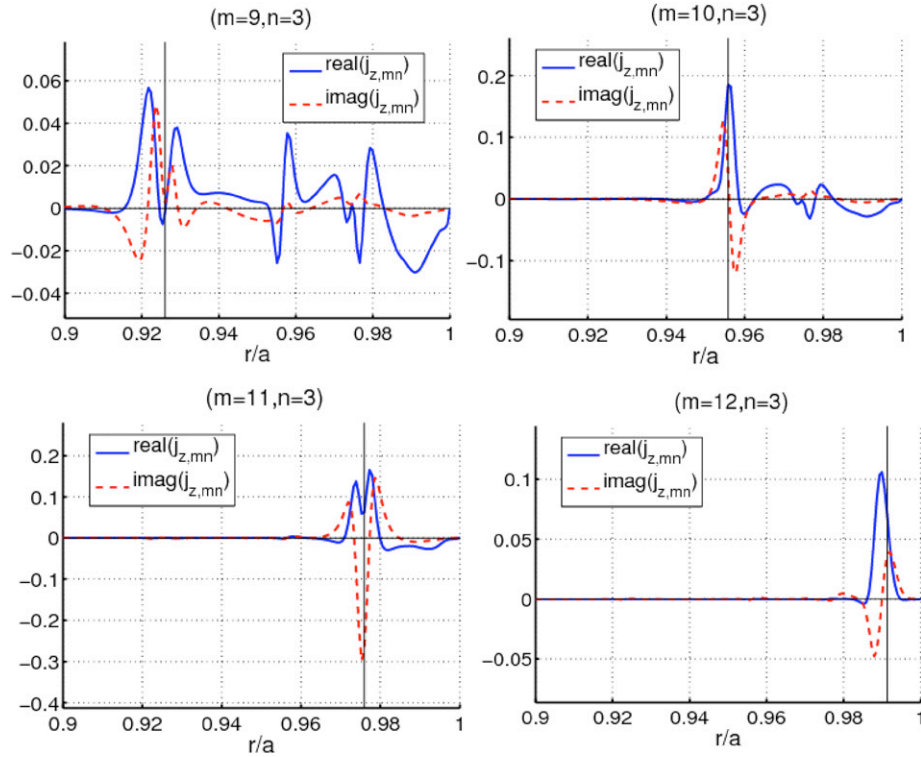
Figure 5. Final profile of the parallel current density for each perturbation harmonic. The position of the resonant surface is shown by the vertical line.
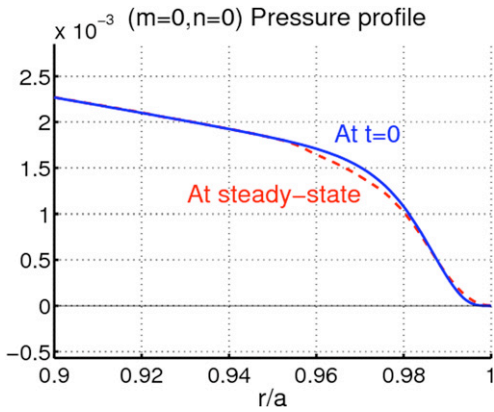

Figure 6. Pressure profiles for the $(m = 0, n = 0)$ harmonic at the beginning and at the end of the simulation.

the electron perpendicular velocity $V_{\perp e}$, or equivalently the quantity $E_r + (\partial_r p_e / e n_e)$: if this is found to vanish at a resonant surface, island penetration could be expected, otherwise a screening should take place.

4. Discussion

The Fitzpatrick theory [8, 9] describes a mechanism for RMP penetration: they induce a $J \times B$ torque (contained in the $\nabla_\parallel J$ term in equation (1)) at the resonant surface, in the opposite direction to the rotation. The torque becomes larger as the rotation slows down, so that if the RMPs are large enough compared with the viscosity (that tends to maintain the rotation), a dramatic braking takes place and the RMPs penetrate.

Our model contains this physics but in the simulation presented in this paper, the RMPs are below the penetration threshold. It can be seen, however, that they modify the rotation. Here, since two-fluid effects are taken into account, by 'rotation' we mean the total perpendicular velocity of the electrons $V_{\perp e} = V_E + V_{*e}$. This can be affected either through the $E \times B$ velocity V_E or through the diamagnetic velocity V_{*e}. The latter may be influenced in particular by the $\beta \nabla_\parallel (2\delta J)$ term in equation (3), as shown in [5]. In figure 2, it appears that V_{*e} is the most affected quantity. This may be attributed to the small ratio $\chi_\perp / \nu_\perp$ [5]. The evolution of V_E, which slightly increases everywhere, is qualitatively (but not quantitatively) consistent with figure 6(*b*) of [26]. The resulting effect on $V_{\perp e}$ is that, at each resonant surface, it evolves towards 0, i.e. the RMPs do brake the electron perpendicular rotation (as found in [5–7]), but not enough to penetrate.

We should remark, however, that given the limitations of our simulations, the RMPs penetration threshold may not be represented correctly. In particular, the unrealistically large viscosity that we had to use in order to avoid the intrinsically unstable mode makes the rotation profile more resilient to changes than it should be, and thereby increases the RMPs amplitude needed for penetration. Also, the fact that we use an unrealistic geometry and current profile and, again, an unrealistically large viscosity, must have an impact on the resonant field amplification of the RMPs by the plasma (which plays a role in their penetration [27]). In any case, from the experimental point of view, the RMPs penetration should correspond to $V_{\perp e}$ (or equivalently $E_r + (\partial_r p_e / e n_e)$) going to 0 at the resonant surfaces. It should thus be possible to tell from experimental measurements whether or not the RMPs penetrate.
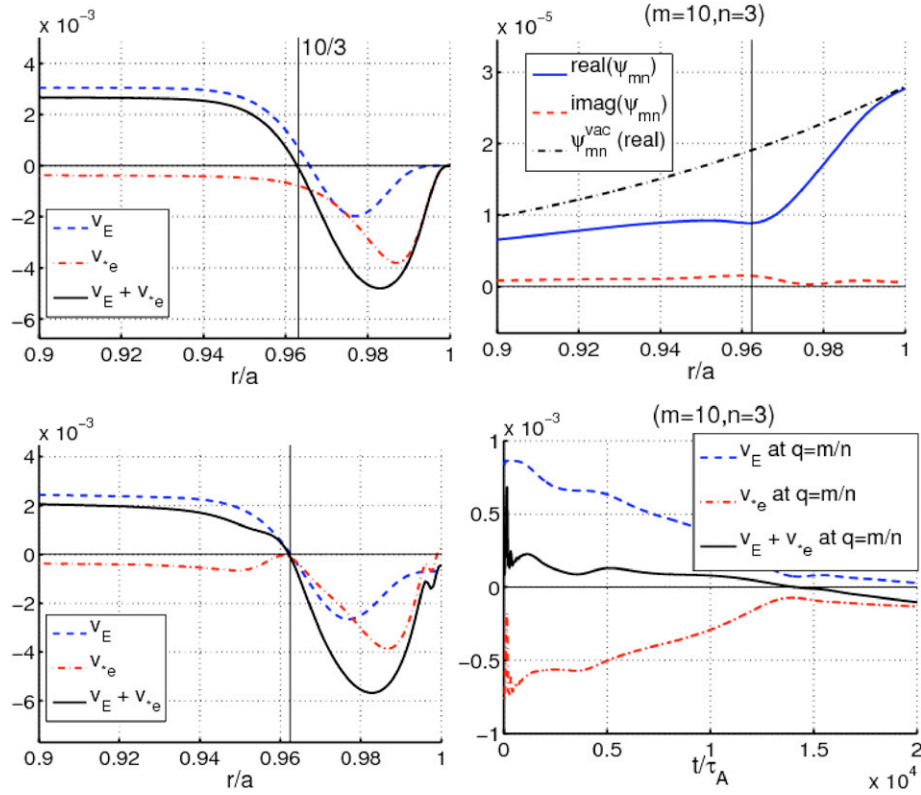
Figure 7. Profiles in the simulation where the current profile was multiplied by 1.03. Top left: input rotation profiles and position of the $q = 10/3$ surface. Top right: final (10, 3) poloidal flux. Bottom left: final rotation profiles. Bottom right: time evolution of the rotation at the $q = 10/3$ surface.

5. Conclusion

The modelling presented in this paper, although highly simplified, retains the main components of the physics of rotational screening of RMPs in the pedestal of an H-mode plasma. Our results indicate that a strong screening takes place over most of the pedestal in the DIII-D ELM control experiments using the I-coils. Only at the very edge (over ∼1% of the normalized radius) is it likely that RMPs penetration takes place and results in a stochastic layer, consistently with the results of Heyn *et al* [14]. Our results put in question the often proposed picture according to which ELM suppression is due to the stochastization of the magnetic field over a region much broader than the pedestal [2]. On the other hand, the screening is consistent with the fact that the electron temperature gradient is not affected by the I-coils experimentally [1]. A transport mechanism due to the RMPs, related to convective cells as well as the screening currents themselves, is found. It appears to be of the same order as the background transport in the pedestal and is therefore a candidate for the experimental density pump-out and changes in the pressure gradient profile. The possibility that an island chain could penetrate on a surface located close to the top of the pedestal is envisaged, but seems inconsistent with experimental observations. Finally, we stress that in our simulations the RMPs are below the penetration threshold, but the model is not solid enough to ascertain this conclusion. We, however, suggest that a careful analysis of the experimental profile of $E_r + (\partial_r p_e / e n_e)$ should give an answer to the question of whether mode penetration occurs or not.

Acknowledgments

Appendix. BC to represent external RMPs

In this appendix, we derive a proper BC to represent RMPs driven by external currents in cylindrical geometry. We assume that the plasma is surrounded by an infinite vacuum with only an infinitesimally thin layer of axial current at a certain radius r_c, with an (m, n) symmetry: $J(r, z, \theta) = I_{mn}/2\pi r_c \cdot \delta(r - r_c) \cdot \exp(im\theta - in(z/R_0))$, where δ denotes the Dirac function.

BC at the coils radius. As a first step, let us assume that we want to know the BC at the radius r_c. We will generalize below to any radius between the plasma and the coils. Integrating Ampère's law across a cylindrical layer around r_c and taking the limit where the layer is infinitesimally thin, we have $[\![\psi'_{mn}]\!]_{r_c} = -\mu_0 I_{mn}/2\pi \cdot r_c$ (1), where $[\![\ ]\!]_{r_c}$ denotes the jump across r_c and the prime corresponds to the radial derivative.

It is easy to show (again by applying Ampère's law, which gives $\Delta_\perp \psi = 0$ in vacuum) that for $r > r_c$, ψ_{mn} has an r^{-m} dependence, provided $m \neq 0$. Therefore, $\psi'_{mn}(r_{c+}) = -(m/r_c)\psi_{mn}(r_c)$, where the LHS designates the limit value as r approaches r_c from $+\infty$. In the RHS, the continuity of ψ_{mn} (which stems from the continuity of the radial magnetic field across the current layer), allows us to write r_c rather than r_{c+}. In a similar way, if there was no plasma, ψ_{mn} (which we denote ψ_{mn}^{vac} in that case) should have an r^m dependence for $r < r_c$, and we would then have $[\![\psi_{mn}^{vac'}]\!]_{r_c} = -(2m/r_c)\psi_{mn}^{\text{vac}}(r_c)$. Thus, $I_{mn} = 4\pi \cdot m \cdot \psi_{mn}^{\text{vac}}(r_c)/r_c$. The correct BC at $r = r_c$ can then be written

$$\psi'_{mn}(r_{c-}) = \frac{m \cdot (2\psi_{mn}^{\text{vac}}(r_c) - \psi_{mn}(r_c))}{r_c}.$$

It is interesting to note that this BC involves both ψ_{mn} and ψ'_{mn}, i.e. it is a mixture of Neumann and Dirichlet conditions.

BC at any radius between the plasma and the coils. Let us now study the more general case where we want a BC at a given radius r_s between the plasma and the coils (in the case of this paper, this radius is actually the plasma radius). For $r \geqslant r_s$, ψ_{mn} is entirely determined by Ampère's law and the following two BCs: $\psi_{mn}(r_s) = \psi_{mn}^s$, where ψ_{mn}^s is not known *a priori*, and $\psi'_{mn}(r_{c-}) = m \cdot (2\psi_{mn}^{\text{vac}}(r_c) - \psi_{mn}(r_c))/r_c$, the relation which we derived above. Since Ampère's law is linear, we can decompose the problem of finding ψ_{mn} into two separate problems for two functions ψ_{mn}^1 and ψ_{mn}^2. We require that these functions satisfy Ampère's law and the BCs: $\psi_{mn}^1(r_s) = \psi_{mn}^s$, $\psi_{mn}^{1'}(r_{c-}) = -m \cdot \psi_{mn}^1(r_c)/r_c$, $\psi_{mn}^2(r_s) = 0$ and $\psi_{mn}^{2'}(r_{c-}) = -((m \cdot (2\psi_{mn}^{\text{vac}}(r_c) - \psi_{mn}^2(r_c)))/r_c)$, ψ_{mn} is then simply obtained by adding ψ_{mn}^1 and ψ_{mn}^2. Now, a few lines of algebra show that $\psi_{mn}^1(r) = \psi_{mn}^s \cdot (r/r_s)^{-m}$ and $\psi_{mn}^2(r) = \psi_{mn}^{\text{vac}}(r_c) \cdot [(r/r_s)^m - (r/r_s)^{-m}]$. Summing the two

and taking the radial derivative at $r = r_s$, we finally obtain the proper BC:

$$\psi'_{mn}(r_{s-}) = \frac{m \cdot (2\psi_{mn}^{\text{vac}}(r_c) \cdot (r_s/r_c)^m - \psi_{mn}(r_s))}{r_s}.$$

Euratom/UKAEA © 2010.

References

[1] Evans T.E. *et al* 2008 *Nucl. Fusion* **48** 024002
[2] Fenstermacher M.E. *et al* 2008 *Phys. Plasmas* **15** 056122
[3] Liang Y. *et al* 2007 *Phys. Rev. Lett.* **98** 265004
[4] Liang Y. *et al* 2007 *Plasma Phys. Control. Fusion* **49** B581
[5] Yu Q. and Günter S. 2009 *Nucl. Fusion* **49** 062001
[6] Yu Q. *et al* 2008 *Nucl. Fusion* **48** 024007
[7] Yu Q. *et al* 2009 *Phys. Plasmas* **16** 042301
[8] Fitzpatrick R. 1993 *Nucl. Fusion* **33** 1049
[9] Fitzpatrick R. 1998 *Phys. Plasmas* **5** 3325
[10] Bécoulet M. *et al* 2008 *Nucl. Fusion* **48** 024003
[11] Nardon E. *et al* 2007 *Phys. Plasmas* **14** 092501
[12] Izzo V.A. and Joseph I. 2008 *Nucl. Fusion* **48** 115004
[13] Strauss H.R. *et al* 2009 *Nucl. Fusion* **49** 055025
[14] Heyn M.F. *et al* 2008 *Nucl. Fusion* **48** 024005
[15] Reiser D. and Chandra D. 2009 *Phys. Plasmas* **16** 042317
[16] Aydemir A.Y. 1992 *Phys. Fluids* B **4** 3469
[17] Schaffer M.J. *et al* 2008 *Nucl. Fusion* **48** 024004
[18] Connor J.W. and Wilson H.R. 2000 *Plasma Phys. Control. Fusion* **42** R1–R74
[19] Stix T.H. 1973 *Phys. Fluids* **16** 1260
[20] Shaing K.C. *et al* 1999 *Phys. Rev. Lett.* **83** 3840
[21] Diamond P.H. *et al* 2005 *Plasma Phys. Control. Fusion* **47** R35–R161
[22] Harvey R.W. *et al* 1981 *Phys. Rev. Lett.* **47** 102
[23] Kaganovich I. and Rozhansky V. 1998 *Phys. Plasmas* **5** 3901
[24] Unterberg B. *et al* 2007 *J. Nucl. Mater.* **363–365** 698–702
[25] Spitzer L. and Härm R. 1953 *Phys. Rev.* **89** 977
[26] Burrell K.H. *et al* 2005 *Plasma Phys. Control. Fusion* **47** B37–52
[27] Park J.K. *et al* 2007 *Phys. Rev. Lett.* **99** 195003